Int. J. Heat Mass Transfer. Vol. 28, No. 12, pp. 2285–2298, 1985
Printed in Great Britain

0017–9310/85 $3.00 + 0.00
Pergamon Press Ltd.

Shock-induced flow in regular arrays of cylinders and packed beds

B. ROGG,* D. HERMANN and G. ADOMEIT
Institut für Allgemeine Mechanik, Rheinisch–Westfälische Technische Hochschule Aachen, Aachen, F.R.G.

(*Received* 20 *December* 1985)

Abstract—Shock-induced flow in a solid matrix consisting of either a packed bed of spherical pellets or an array of cylinders perpendicular to the flow is investigated experimentally and numerically. The experiments are performed in a shock tube measuring pressure profiles in front of and within the solid matrix. Qualitative information on the flow pattern in the array of cylinders is obtained from shadowgraphs. In the numerical calculations various drag and heat-transfer laws are tested. Tentative adjustments of these correlations are made to fit the numerical results to the experimental data.

1. INTRODUCTION

THE FLOW of non-reacting gases through packed beds is characterized by the momentum and energy exchange between the gas phase and the solid phase. Both phenomena have been investigated by numerous researchers who have attempted to determine fundamental coefficients of drag and heat transfer based on the properties of the fluid and the solid. A great deal of effort has been devoted to establish flow-resistance correlations which are valid for wide ranges of Reynolds numbers. Since the formula given by Ergun in 1952 [1] turned out to give the best agreement with a variety of experimental data it has been adopted and commonly used during the last three decades. Another correlation—to be used preferably for packed beds consisting of spherical pellets—was given by Brauer [2] in 1960. A new drag correlation was introduced by Kuo and Nydegger [3] in 1978 and another by Jones and Krier [4] in 1983. The last one, however, essentially confirms the correlation given earlier by Brauer. Although both new correlations differ the common conclusion of their investigators is that the extrapolation of Ergun's formula to higher Reynolds numbers is not permissible.

Extended experimental studies on the heat transfer in packed beds have been performed, e.g. [5–9]. Similar to the difficulties in the determination of flow-resistance correlations, the major problem consisted in finding suitable correlations between a non-dimensional heat-transfer coefficient, a Reynolds number and a Prandtl number. Today it is preferable to use the correlations of Denton [7], Yoshida *et al.* [8] and Gnielinski [9].

All studies cited above refer to steady and isothermal flow conditions. However, unsteadiness of the flow may become important, e.g. when the flow is induced by a shock wave. This was found by Heilig and Reichenbach [10, 11] who investigated experimentally the flow resistance of a single cylindrical body. They found that the drag coefficient is strongly time dependent and its value can exceed the steady-state value by a factor of up to 30, depending on Mach and Reynolds numbers. Zloch [12] used a shock tube to generate shock-induced flow in an array of axially arranged tubelets. He investigated experimentally and numerically the decrease of the shock strength within the obstacles. By making the area change rather large, he considered only the special case of steady-state boundary conditions at the entrance into the tubelets. In the numerical calculations he employed the laws of turbulent pipe flow to describe the momentum and heat transfer between the phases.

In the present paper shock-induced flow in a solid matrix is studied experimentally and theoretically. The experiments were performed in a shock tube taking as matrix either a packed bed or an array of cylinders with their axis perpendicular to the flow axis. Pressure profiles are measured in dependence upon time and location in front of and within the matrix. In the array of cylinders shadowgraphs are also taken to obtain qualitative information on the shock-induced flow and wave patterns. These data are compared with numerical results obtained by solving the basic equations using a method of characteristics. Particular account was taken of coupling the regions of flow in front of and within the matrix. Flow-resistance and heat-transfer correlations of different authors have been varied systematically.

2. EXPERIMENTS

2.1. *Experimental methods and apparatus*

The experiments were carried out in a conventional pressure-driven shock tube (Fig. 1) with a rectangular cross-section of 54 × 54 mm, using nitrogen as the test gas. In the test section, located at the end of the shock tube, as a solid matrix both packed beds of spherical

* Present address: Institut für Angewandte Physikalische Chemie, Universität Heidelberg, Im Neuenheimer Feld 253, 69 Heidelberg, F.R.G.

NOMENCLATURE

A	cross-sectional area [m^2]
c	specific heat [$J\ kg^{-1}\ K^{-1}$]
d	diameter [m]
f, F	non-dimensional friction coefficients, defined by equations (11) and (12)
l	length of the packed bed [m]
M_0	Mach number of the incident shock
Nu	Nusselt number
p	pressure [$N\ m^{-2}$]
Pr	Prandtl number
q	flow rate [$m^3\ s^{-1}$]
Q	heat flux, defined by equation (5) [$W\ m^{-3}$]
Re	Reynolds number
s	specific wetted surface area of packed bed, defined by equation (6) [m^{-1}]
t	time coordinate [s]
T	temperature [K]
T_0	reference temperature, equal to 300 K
u	velocity [$m\ s^{-1}$]
x	space coordinate [m].

Greek symbols

α	heat-transfer coefficient [$W\ m^{-2}\ K^{-1}$]
β	drag force, defined by equation (4) [$N\ m^{-3}$]
Δp	overall pressure loss [$N\ m^{-2}$]
γ	ratio of specific heats c_p and c_v
ε	porosity, volume fraction of void
λ	thermal conductivity [$W\ m^{-1}\ K^{-1}$]
η	dynamic viscosity [$N\ s\ m^{-2}$]
ρ	density [$kg\ m^{-3}$]
ω	exponent.

Subscript

s	solid.

glass pellets (diameter 4, 5, 6 and 8 mm) and arrays of cylinders (diameter 5, 10 and 30 mm) arranged perpendicular to the tube axis were investigated. The resulting wave system and the pressure distribution for these arrangements are represented schematically in Fig. 2. Note that Fig. 2 gives only a strongly simplified representation; the real flow and wave pattern is rather complex and will be discussed below on the basis of the shadowgraphs.

In the shock tube a plane shock wave, running with constant velocity was generated. The Mach number of the incident shock wave was determined using film

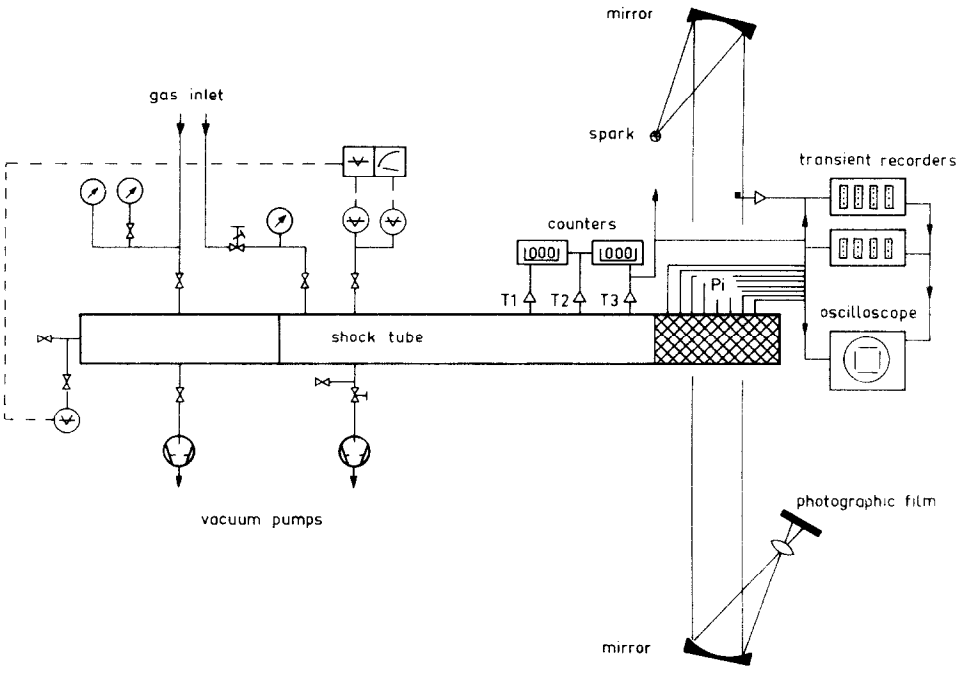

FIG. 1. Schematic diagram of the shock-tube arrangement.

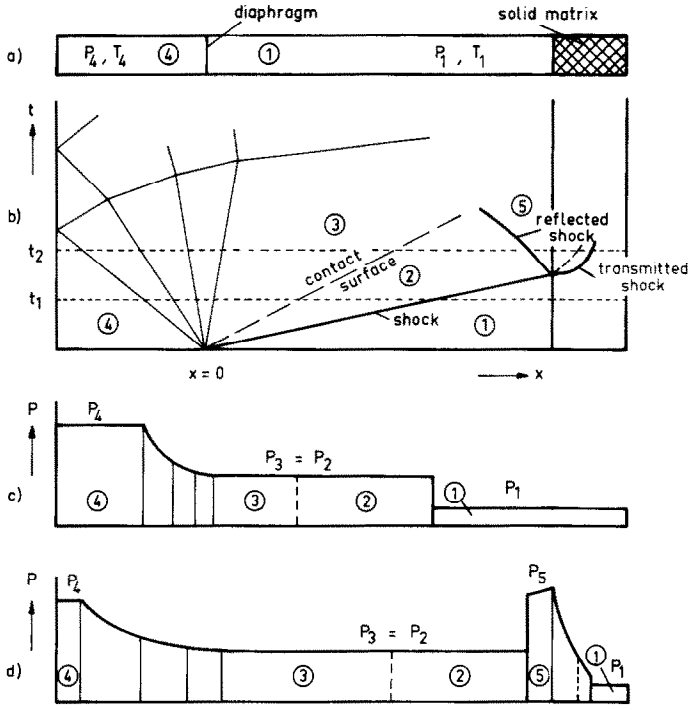

FIG. 2. Schematic representation of: (a) shock tube with test section; (b) wave diagram; (c) pressure profile before shock's impingement on the solid matrix ($t = t_1$); (d) pressure profile after shock's impingement on the solid matrix ($t = t_2$).

temperature gages. At several locations inside and in front of the solid matrix pressure profiles were measured using gages of the type Kistler 603 B, 6031 and Piezotronics 113 A 21, 113 A 24. The pressure gages were installed in the tube wall. Optical informations on the flow and wave pattern were obtained taking shadowgraphs by using either a single spark or a Cranz–Schardin multiple spark arrangement.

2.2. *Experimental results*

Prior to discussing the experimental results we give a brief description of the wave processes. The shock wave impinging on the solid matrix is partially transmitted and partially reflected by the elements. At the entrance into the matrix the transmitted shock wave is accelerated due to the area reduction, further inside it is weakened very rapidly. In opposition to this, the reflected shock wave is accelerated and therefore strengthened with growing time. The individual processes are very complex and will be shown below in the shadowgraphs of Fig. 6. A first strong reflection is followed by further weaker reflections which lead to the acceleration of the reflected shock and to a pressure increasing with time in front of the solid matrix (region 5 of the wave diagram in Fig. 2).

Some of the experimental results are represented in Figs. 3–7.

Figures 3–5 refer to the fixed bed and Figs. 6 and 7 to the arrays of cylinders. Figure 3 shows some typical pressure records obtained for a packed bed. The pressure gages 3–5 were located 22.5–72.5 mm in front of and gages 6–8, 25.5–72.5 mm inside the bed. Probe 6, 25.5 mm inside the bed, shows three distinctive pressure peaks which indicate shock waves, whereas probe 8, 72.5 mm inside the bed, shows already an essentially continuous pressure increase. Plotting the pressure measured by the different gages at fixed times vs location the representations shown in Figs. 4 and 5 are obtained (for another representation see Fig. 19 in the theoretical part). The parameters varied in Figs. 4 and 5 are the diameter of the spherical pellets and the Mach number of the incident shock. It may be seen that the pressure level in front of the bed increases with decreasing diameter of the pellets and increasing Mach number approaching in the limit the value which would be reached if the incident shock wave were reflected at a solid end wall.

Results obtained for arrays of cylinders are represented in Figs. 6 and 7. Shadowgraphs of the resulting wave and flow pattern in an array of cylinders taken at distinctive moments are shown in Fig. 6. Its various features may be essentially explained by comparison with results obtained for single cylinders [10, 11]. Remarkable is the strong effect of the boundary layer along the front part of the cylinders upon the light refraction and also the formation of dual

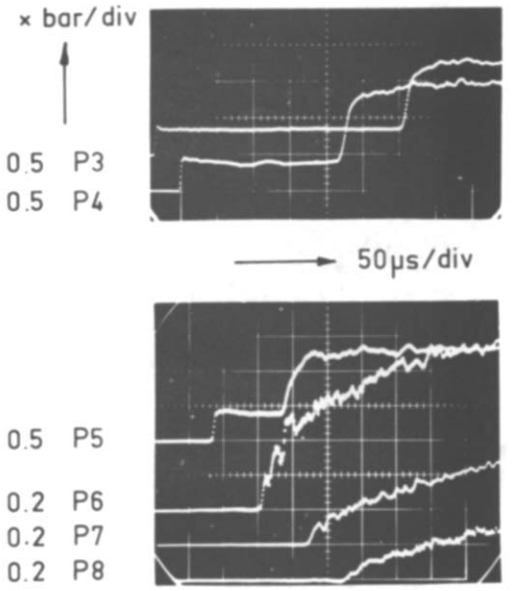

FIG. 3. Pressure records of gages 3–5 in front of and 6–8 within the packed bed. (Glass beads 8 mm ∅, porosity $\varepsilon = 0.395$, driven gas N_2, $M_0 = 2.05$, $p_1 = 0.1$ bar, $T_1 = 296$ K.)

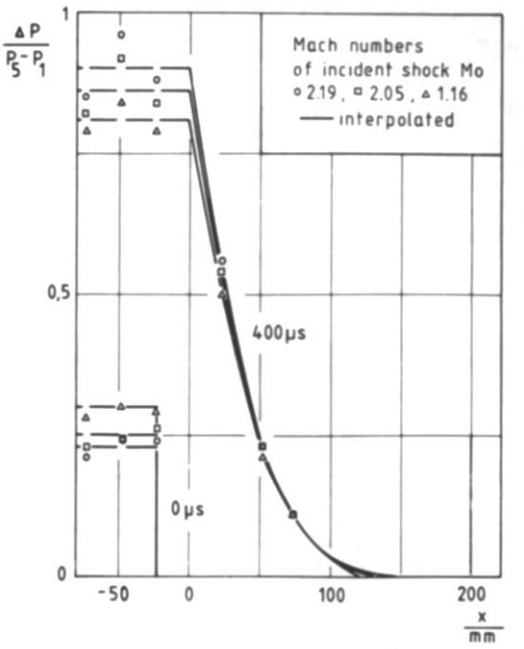

FIG. 5. Measured pressure p vs location x for various Mach numbers M_0 of the incident shock. (Glass beads 6 mm ∅, driven gas N_2, $p_1 = 0.1$ bar, $T_1 = 296$ K.)

vortices behind the obstacles. Between the cylinders of the first row a supersonic jet is formed which temporarily leads to a bow shock wave in front of the cylinders of the following row. Jet and recirculation regions are separated by a clearly visible shear layer, e.g. in the third photograph of Fig. 6. The pressure records

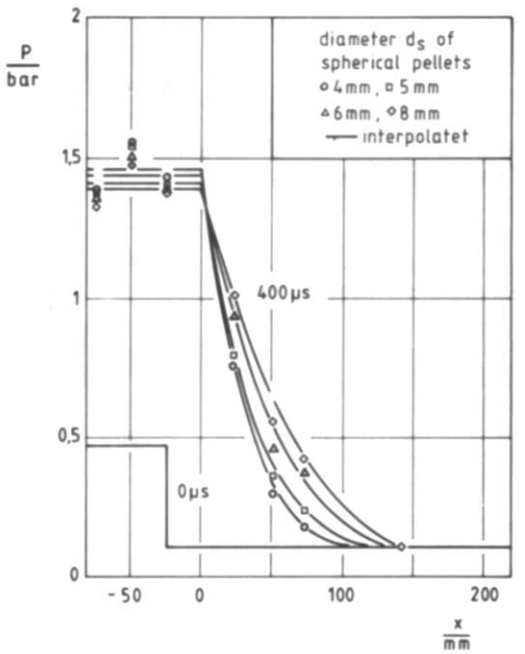

FIG. 4. Measured pressure p vs location x for various diameters d_s of pellets. (Glass beads, driven gas N_2, $M_0 = 2.05$, $p_1 = 0.1$ bar, $T_1 = 296$ K.)

(pressure gages installed in the tube wall) obtained at the locations 4–13 as indicated are also shown in Fig. 6. The pressure gages 4 and 5 located in front of the array of cylinders show the incident shock wave and a first strong reflected shock wave which is followed by several weaker reflected waves. At probes 6–13 located inside the array various waves may be clearly distinguished. The strength of the transmitted shock wave and the pressure value further inside decreases very rapidly; but, due to the interaction of several waves, locally high pressure peaks are possible.

The experiments with the array of cylinders have been performed for various cylinder sizes with diameters of 5, 10 or 30 mm in geometrically similar arrangements, but with the porosity held fixed at a value of 0.72. Figure 7 shows shadowgraphs of the array of cylinders with diameters of 30 mm. A comparison shows that there is a very good agreement between the wave patterns for the different cylinder sizes. However, from the arrangements with the cylinders of 30 mm in diameter more detailed information may be obtained. A comparison of the pressure records obtained for the arrays of cylinders in geometrically similar arrangements shows extensive agreement for the various cylinder sizes even in details (these pressure records are not shown here). Pressure measurements at a reduced porosity of 0.44 show that at the beginning of the array pressure peaks locally exceed the value which would be reached if the incident shock wave were reflected at a solid end wall.

After a short time, when the flow processes become dominant, these phenomena disappear. Shadow-

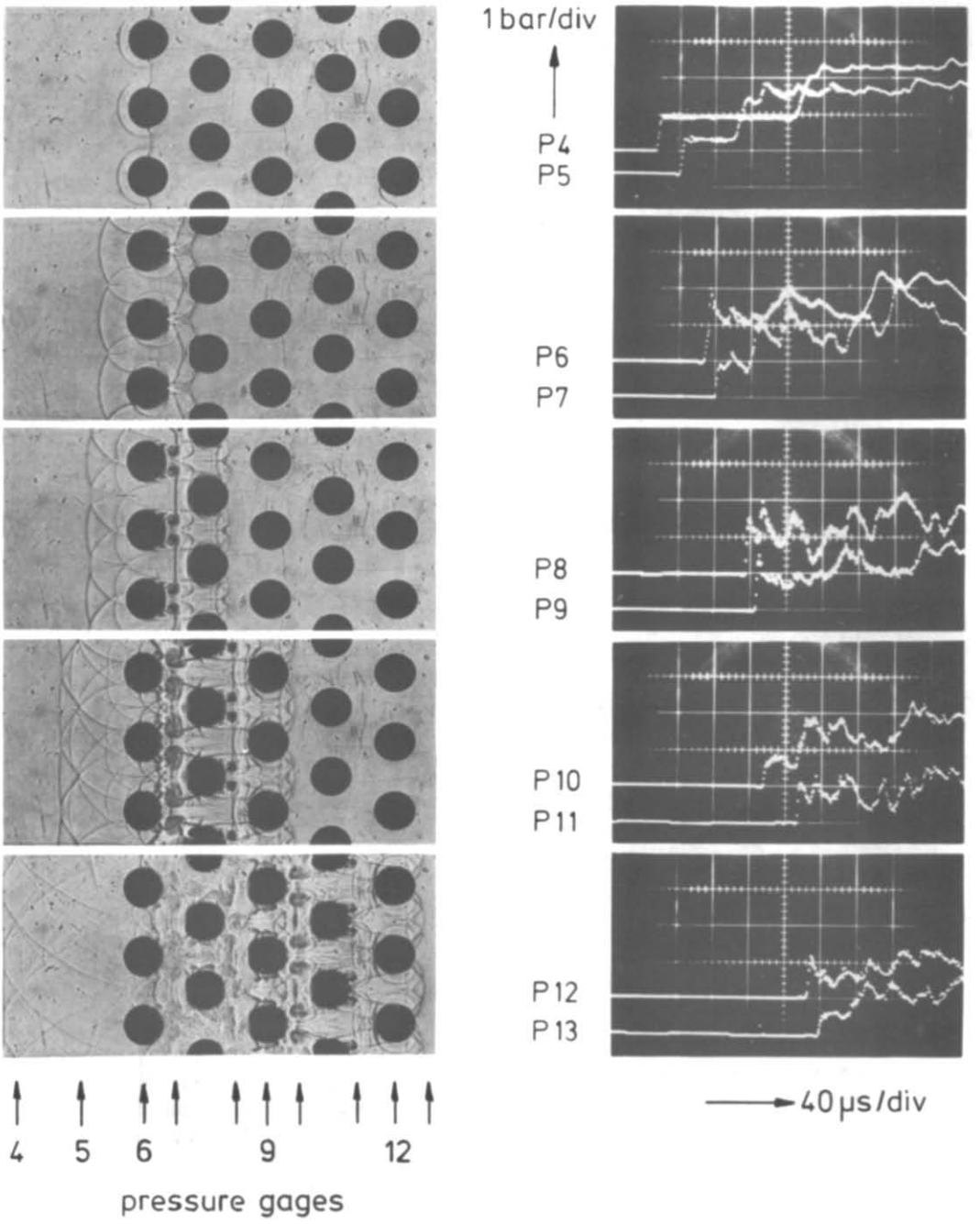

FIG. 6. Left column : shadowgraphs of a shock wave, approaching from the left and impinging on an array of cylinders with their axis perpendicular to the shock-tube axis. Time of the single shadowgraphs, referred to the time when the incident shock wave passes gage 5 : $t = 27\,\mu s, 45\,\mu s, 61\,\mu s, 90\,\mu s, 151\,\mu s$. Right column : pressure records of the gages 4–13, arranged corresponding to the left photograph. (Cylinders 10 mm ∅, porosity $\varepsilon = 0.72$, driven gas N_2, $M_0 = 1.74$, $p_1 = 0.4$ bar, $T_1 = 295$ K.)

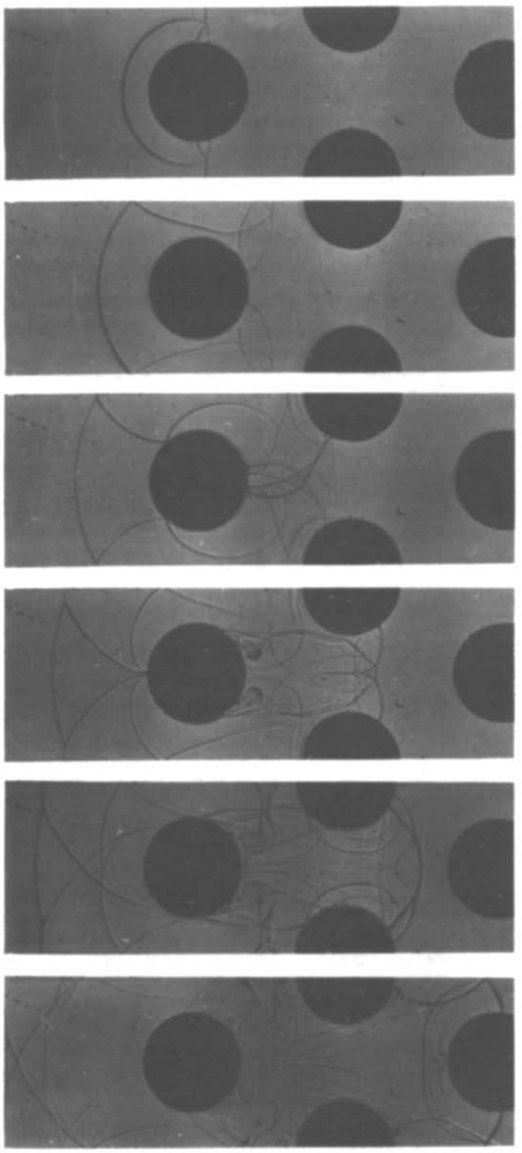

FIG. 7. Shadowgraphs of a shock wave, approaching from the left and impinging on an array of cylinders with their axis perpendicular to the shock tube axis. Driven gas N_2, cylinders 30 mm $\varnothing$, $\varepsilon = 0.72$, $M_0 = 1.68$, $p_1 = 0.4$ bar, $T_1 = 293$ K. Time of the single shadowgraphs, referred to the time when the incident shock wave passes gage 5 (corresponding to Fig. 6); $t = 80, 112, 144, 176, 200, 249$ μs.

graphs, not given here, show that the flow field becomes wholly turbulent after very short times. Particularly the pressure measurements made in packed beds as represented in Figs. 4, 5 and 19 should belong to this regime.

3. THEORY

3.1. *Governing equations*

Inside the solid matrix, the flow and wave pattern is three-dimensional. Since the complete analysis of this problem is not the goal of this paper, at the present time an unsteady one-dimensional approach is used. Such a formulation of the problem (with the only spatial coordinate being parallel to the shock-tube axis) may be understood as resulting from the three-dimensional Navier–Stokes equations by integrating those in the transverse directions. Even though important details about the wave and flow processes (e.g. interaction of waves, structure of boundary layers, formation of vortices) are lost by integrating over the transverse space dimensions, essential overall features of the processes may be retained by introducing appropriate interaction terms into the one-dimensional balance equations. Relations of this type have been derived and used in various investigations (cf. refs. [13, 15, 17]). Here in the set of balance equations for the unsteady one-dimensional two-phase flow the velocity of the solid phase is taken to be zero and heat loss to the tube wall, friction force exerted on the gas by the tube wall, viscous dissipation in the gas phase, heat conduction in the gas phase, and the temperature dependence of the specific heats are neglected.

After rearranging various terms and inserting the perfect-gas law the following set of partial differential equations is obtained [13, 14, 19]:

$$\frac{\partial \rho}{\partial t} + u\frac{\partial \rho}{\partial x} = -\rho\frac{\partial u}{\partial x}, \tag{1}$$

$$\frac{\partial u}{\partial t} + u\frac{\partial u}{\partial x} = -\frac{1}{\rho}\left(\frac{\partial p}{\partial x} - \beta\right), \tag{2}$$

$$\frac{\partial p}{\partial t} + u\frac{\partial p}{\partial x} = -\gamma p\frac{\partial u}{\partial x} - (\gamma - 1)(Q + \beta u). \tag{3}$$

The heat flux Q and the drag force β are defined as [15, 19]:

$$\beta \equiv -\frac{s\varepsilon^2}{3(1-\varepsilon)}\rho u^2 f, \tag{4}$$

$$Q \equiv \frac{s}{\varepsilon}\alpha(T - T_s). \tag{5}$$

For spherical pellets the specific surface s is [15]:

$$s = \frac{6(1-\varepsilon)}{d_s}. \tag{6}$$

Under the assumption of a uniform pellet temperature an energy balance leads to the following ordinary differential equation for the temperature of the particles:

$$\frac{\partial T_s}{\partial t} = \frac{\varepsilon}{1-\varepsilon}\frac{Q}{\rho_s c_s}. \tag{7}$$

These equations are used to describe the flow inside the packed bed. The same equations—setting $\beta = Q = 0$—are used to describe the flow in the upstream region in front of the packed bed. These two regions are coupled by:

—the energy equation for quasi-steady flow of perfect gas

$$\frac{\gamma}{\gamma - 1}p/\rho + u^2/2 = \text{const.}, \tag{8}$$

—the isentropic law

$$p/\rho^{\gamma} = \text{const.}, \tag{9}$$

—and the continuity equation for quasi-steady flow

$$\rho u A = \text{const.} \tag{10}$$

The applicability of these equations as coupling conditions rests upon the fact that the extension of the transition zone between packed bed and free flow is small compared to the characteristic length of the problem. These conditions have for example been discussed by Laporte [16]. They establish a dependence between porosity ε, the states in front of the incident shock wave and the Mach numbers of the incident, reflected and transmitted shock waves.

3.2. *Flow-resistance and heat-transfer correlations*

The friction coefficient f is defined as [15]

$$f = \frac{\Delta p}{l}\frac{d_s}{\rho u^2}\frac{\varepsilon}{1-\varepsilon}. \tag{11}$$

In some cases it is convenient to use an inverse drag coefficient F which is related to f by

$$F = 2 f Re_s \varepsilon^3/(1-\varepsilon)^2. \tag{12}$$

Here the Reynolds number Re_s is defined as

$$Re_s = \varepsilon \frac{\rho u d_s}{\eta}. \tag{13}$$

References [2–4, 15] give reviews of the important literature on the dependence of the overall pressure loss upon the steady flow properties. In the present paper the flow-resistance laws given by Brauer [2], Ergun [1], Kuo and Nydegger [3] and Jones and Krier [4] were used. The correlations and their validity ranges are given in Table 1. In Fig. 8 the four correlations are compared graphically. In the whole range of Reynolds numbers the values of the friction coefficient predicted by the Kuo–Nydegger correlation exceed those predicted by the correlation of Jones and Krier. For high Reynolds numbers these two correlations predict lower values for the drag than Ergun's correlation, and vice versa for low Reynolds numbers. Obviously, the Jones–Krier correlation does not differ very much from a correlation given earlier by Brauer.

The non-dimensional heat transfer coefficient is related to the Reynolds and Prandtl numbers. In the present paper the correlations given by Denton [7], Yoshida *et al.* [8] and Gnielinski [9] were used. These correlations and their validity ranges are given in Table 2. In Fig. 9 their Nusselt numbers are plotted as a function of a reduced Reynolds number. It may be seen from the graphs that for high Reynolds numbers the heat-transfer rate predicted by Denton's correlation exceeds the value predicted by Yoshida *et al.* up to a factor of 2, whereas Gnielinski's formula predicts values in between.

3.3. *Results and discussion*

The above equations have been solved numerically using the method of characteristics. The characteristics, the shock waves and the contact surface are represented in Figs. 10 and 11, which exhibit the general features of the flow process. The initial acceleration of the transmitted shock wave due to the area contraction at the beginning of the matrix ($x = 0$), clearly marked by a sharp downward bend, is followed by a deceleration well legible from the upward bend of the shock's pathway. The slight downward bend of the reflected shock's pathway indicates its gradual acceleration due to the increasing obstruction of the solid matrix with increasing time. In Fig. 10 the particle pathlines and in Fig. 11 the left- and right-running Mach lines are plotted. The sharp bend of the particle pathlines at the beginning of the matrix indicates the strong acceleration of the gas due to the area contraction. From the slopes of the left-running Mach lines it may be gathered that—in the case considered—the flow behind the transmitted shock wave is initially supersonic and becomes subsonic only when the shock wave has already been attenuated.

In Figs. 12–14 profiles obtained for pressure, temperature and flow velocity are plotted vs coordinate x at distinctive time intervals after shock impingement upon the solid matrix. The profiles are computed taking the pressure-loss correlation of Ergun [1] and the heat-transfer correlation of Yoshida *et al.* [8] into account. The features of the flow process can be studied. Due to the obstruction of the matrix with increasing time a

Table 1. Flow-resistance correlations with validity ranges

Investigator	Range of Reynolds number	Range of porosity	Correlation	Remarks
Ergun [1, 15]	0.4–1380	0.4–0.65	$F = 150 + 1.75\, Re_s/(1-\varepsilon)$	various shaped particles gas, liquid
Brauer [2, 17]	0.02–18000	0.345–0.421	$F = 160 + 3.1[Re_s/(1-\varepsilon)]^{0.9}$	spheres gas, liquid
Kuo and Nydegger [3]	460–14600	0.38–0.39	$F = 276 + 5.05[Re_s/(1-\varepsilon)]^{0.87}$	ball propellant grains gas
Jones and Krier [4]	440–76000	0.38–0.44	$F = 150 + 3.89[Re_s/(1-\varepsilon)]^{0.87}$	spheres gas

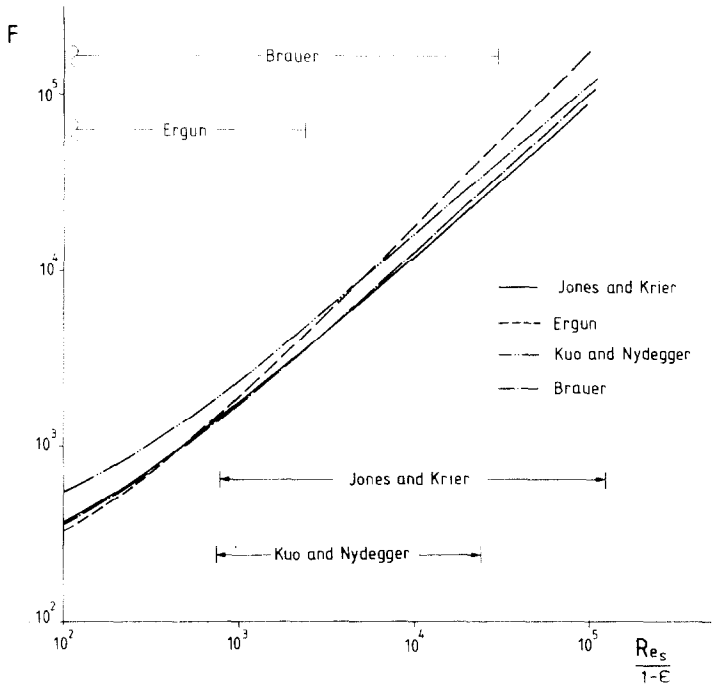

FIG. 8. Graphic representation of the flow-resistance correlations listed in Table 1.

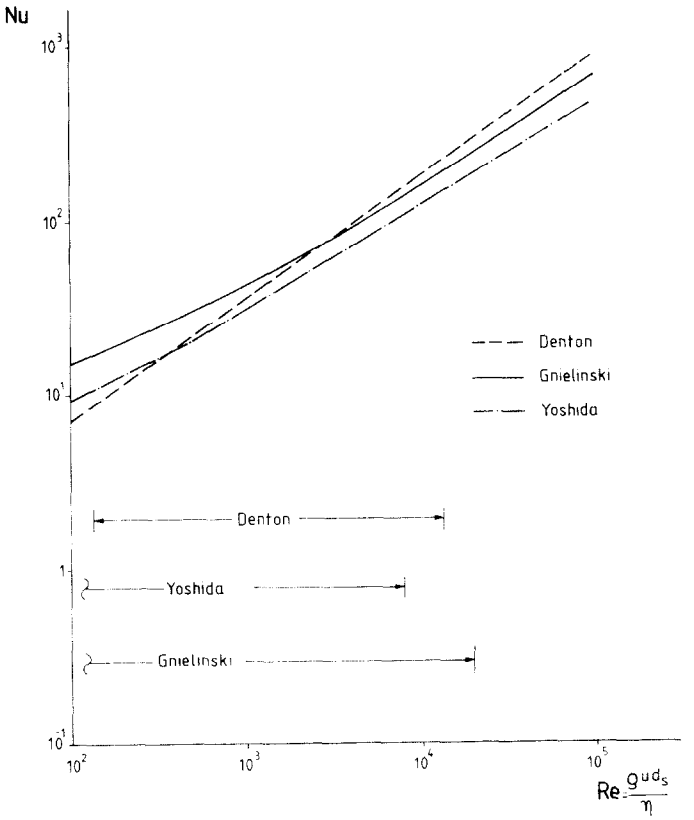

FIG. 9. Graphic representation of the heat-transfer correlations (for $\varepsilon = 0.37$, $Pr = 0.7$) listed in Table 2.

Table 2. Heat-transfer correlations with validity ranges

Investigator	Range of Reynolds number	Range of Prandtl number	Range of porosity	Correlation $Nu = (\alpha d_s/\lambda)$	Remarks
Denton [7, 18]	50–5000	>0.5	0.37	$Nu = 0.8\, Re_s^{0.7}\, Pr^{1/3}$	spheres, any fluid
Yoshida *et al.* [8, 15]	0.1–8000	0.1–0.6 for gases 2–400 for liquids	0.35–0.43	$Nu = a f_\varepsilon^b Re^{1-b} Pr^{1/3}$, where $f_\varepsilon = \frac{6(1-\varepsilon)\psi}{\varepsilon^{b+1}}$ $Re = (\rho u d_s)/\eta$ and $a = 0.91$, $b = 0.51$ for $0.1 < Re \lesssim 400$ $a = 0.61$, $b = 0.41$ for $400 \lesssim Re < 8000$ $\psi = 1$: spheres $\Psi = 0.91$: cylinders	spheres, cylinders, flakes, irregular granules, any fluid
Gnielinski [9]	5–20000	0.7–10000	0.26–0.935	$Nu = f_\varepsilon[2+(Nu_{lam}^2 + Nu_{tur}^2)^{1/2}]$, where $f_\varepsilon = 1+1.5(1-\varepsilon)$ $Nu_{lam} = 0.664\, Re^{1/2} Pr^{1/3}$ $Nu_{turb} = \frac{0.037\, Re^{0.8} Pr}{1+2.443\, Re^{-0.1}(Pr-1)}$	spheres gas, liquid

continuous increase of pressure and temperature and a decrease of velocity is observed between the reflected shock wave propagating to the left and the front of the matrix. At the front itself the gas obeys the balance equations formulated in equations (8)–(10) resulting in an acceleration of the flow in a zone assumed here to be infinitely thin. This leads to the discontinuous changes of the variables of state at $x = 0$, causing the observed drops of pressure and temperature. After the initial acceleration due to the area contraction the transmitted shock wave is attenuated considerably by the drag force β. At the contact surface, originally separating the matrix and the gas outside, a jump and a pronounced peak in temperature are observed.

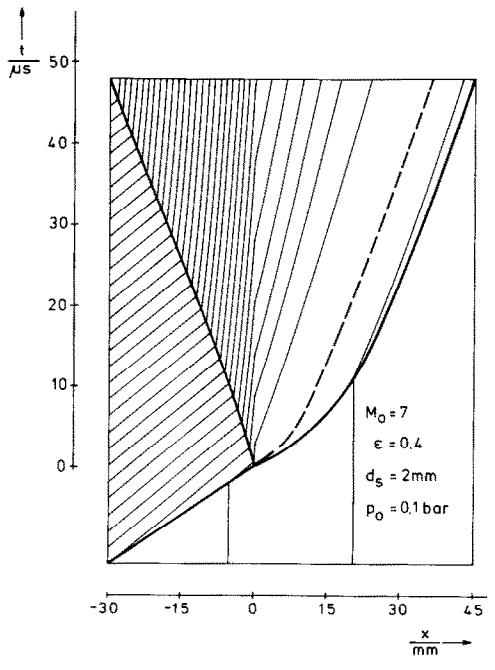

FIG. 10. Wave diagram numerically computed: shocks (thick solid lines), contact surface (dashed line) and particle pathlines (thin solid lines) in front of and inside a packed bed.

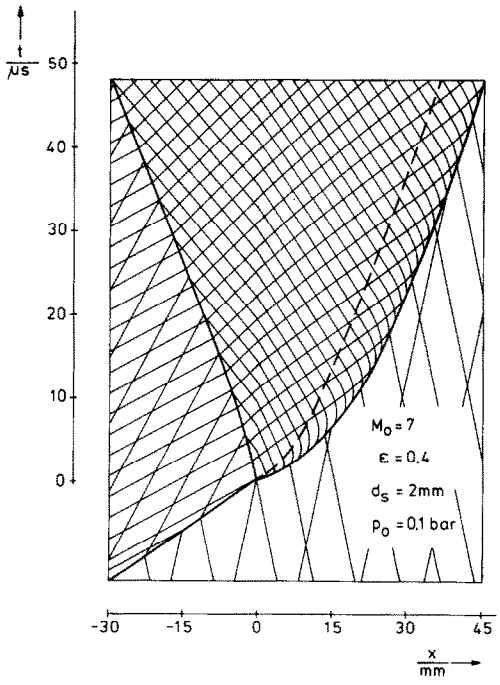

FIG. 11. Wave diagram numerically computed: shocks (thick solid lines), contact surface (dashed line) and Mach lines (thin solid lines) in front of and inside a packed bed.

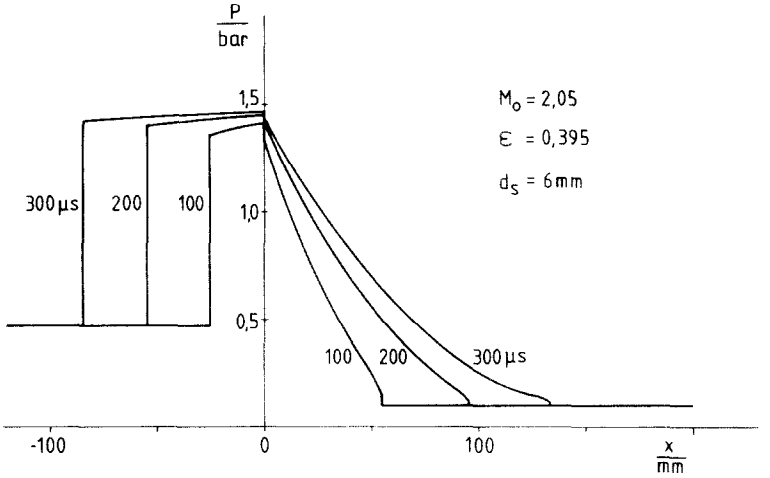

FIG. 12. Development of pressure profiles with time obtained by numerical integration.

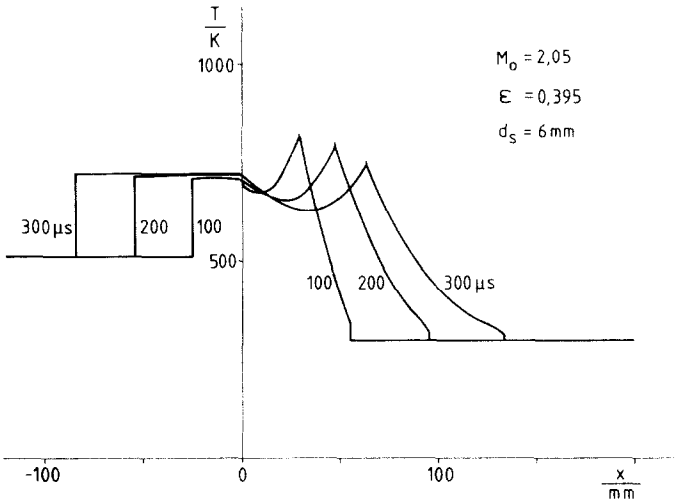

FIG. 13. Development of temperature profiles with time obtained by numerical integration.

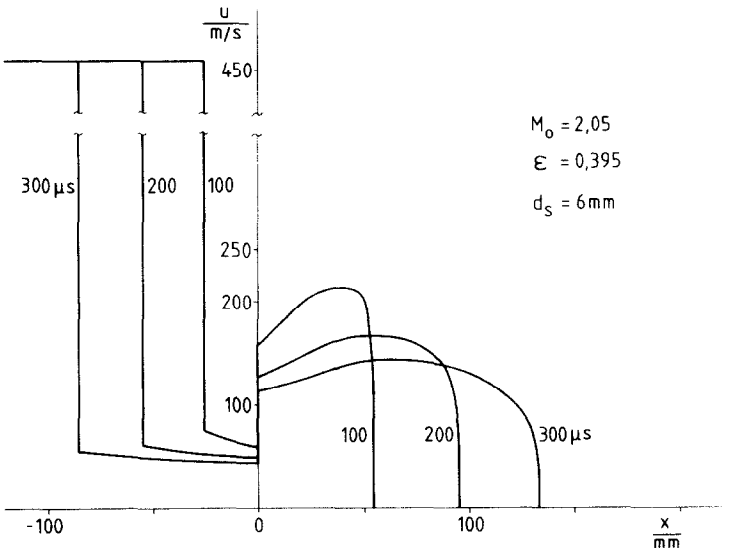

FIG. 14. Development of velocity profiles with time obtained by numerical integration.

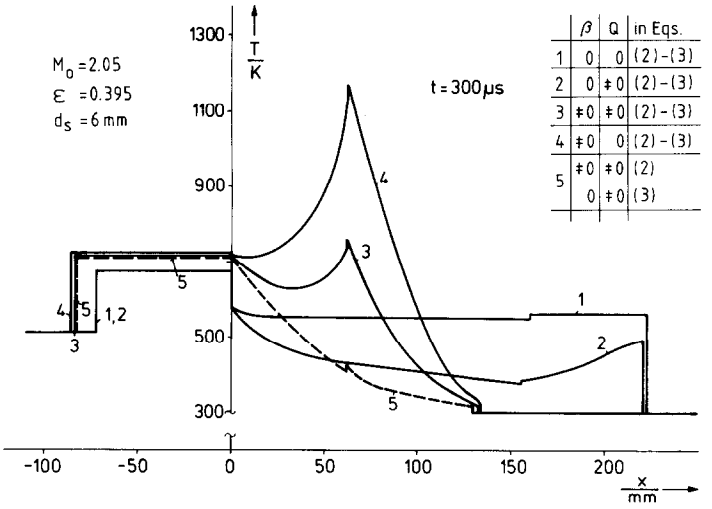

FIG. 15. Numerical solution of T vs x for various values of β and Q.

In Fig. 15 the various influences contributing to this effect can be studied. Here the temperature profiles are plotted vs x for a fixed time interval introducing various values for the drag β and the heat transfer Q. A comparison between curves 1 and 2 shows that the heat flux Q gives only a small contribution to the reduction of the shock strength. The comparison between curves 1 and 2 on the one side and 3 to 5 on the other side shows that this reduction is essentially due to the drag force term in the balance of momentum [equation (2)]. Curves 3 and 5 differ in the presence of the drag force term in the energy balance [equation (3)], which represents the heat dissipation caused by the flow resistance of the solid matrix. It can be gathered that this term causes the temperature increase in the flow field. The maximum temperature itself occurs in the environment of the contact surface since the gas located here has the longest heating time since shock impingement. First experiments to measure this strong local temperature increase being caused by the dissipation of kinetic flow energy have not been successful so far. This may indicate that this kinetic flow energy is transformed in a first step into turbulent kinetic energy and only later dissipated into thermal energy. If this is to be taken into account, equations (1)–(3) must be supplemented by the balance equations of turbulent kinetic energy, e.g. by making use of the k–ε model.

Figure 16 shows the pressure profiles corresponding to the temperature profiles of Fig. 15 exhibiting again the strong difference in shock attenuation caused by the drag force in the momentum equation.

The numerical solutions have also been compared with the experimental results. It was found that the drag and heat-transfer correlations tested lead to pronounced deviations between experiment and theory. The differences resulting from the utilization of different correlations are exhibited in Figs. 17 and 18. Here the computed pressure profiles are plotted for a fixed time interval of 1200 μs after shock impingement on the solid

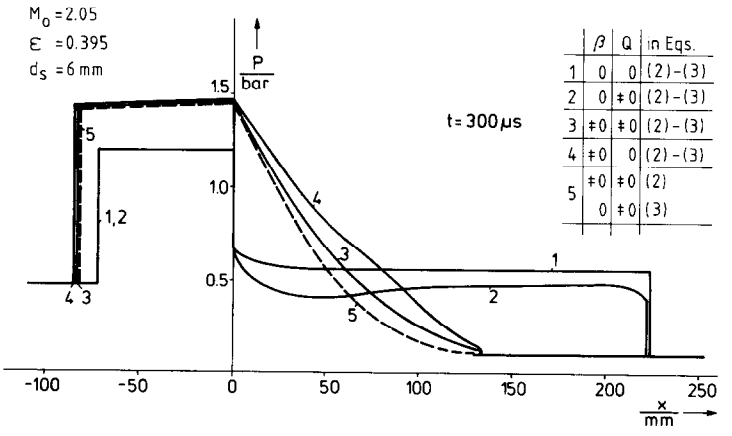

FIG. 16. Numerical solution of p vs x for various values of β and Q.

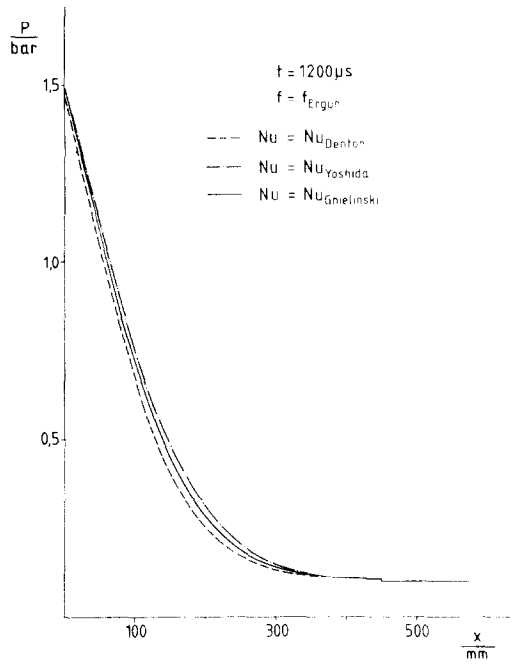

FIG. 17. Pressure profiles obtained by numerical computation using different heat-transfer correlations.

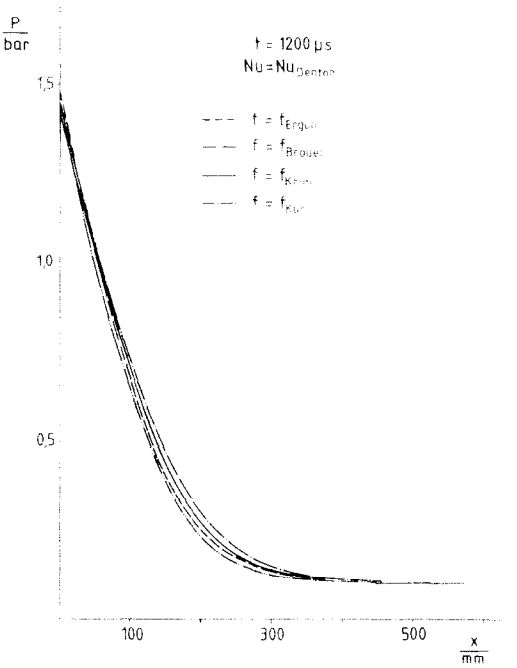

FIG. 18. Pressure profiles obtained by numerical computation using different flow-resistance correlations.

matrix. All curves in Fig. 17 have been computed using Ergun's flow-resistance formula but taking a different heat-transfer law for each curve. Similarly, all curves in Fig. 18 have been computed using Denton's heat-transfer law but employing a different flow-resistance correlation in each case. A comparison of these results with Figs. 8 and 9, respectively, reveals that—as is to be expected—the heat-transfer formulas predicting higher heat-transfer rates predict lower pressure profiles and, similarly, the flow-resistance laws predicting higher drag forces predict lower pressure profiles as well. A comparison of the pressure profiles measured inside the packed bed to the numerical solutions reveals that acceptable agreement between both can only be achieved by adjustments of the empirical drag and heat-transfer correlations. It was found that two kinds of modification are possible, both leading to quantitatively similar results. One possibility is to multiply the drag force predicted by Ergun's formula by a factor of 1.5 and the heat-transfer rate predicted by Yoshida's formula by a factor of 4.

As may be gathered from Fig. 19, this rough procedure leads to acceptable agreement for the pressure distribution inside the packed bed, however, not in front of the matrix. Since the numerical results revealed that the drag force predicted by the original

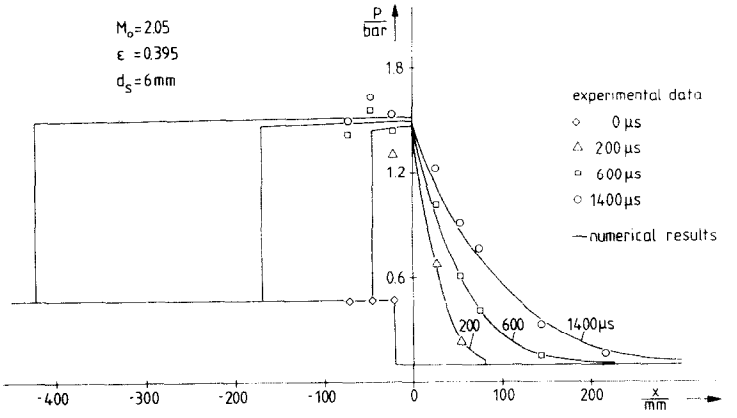

FIG. 19. Pressure p vs location x for various times t. Points: measurements. Solid curves obtained by numerical solution adjusting β and Q.

correlations in the hot flow regions is too low to fit the experimental data, a temperature dependent adjustment of the flow-resistance correlations has been chosen. It was found that a result very similar to the curves already depicted in Fig. 19 may be obtained by multiplying Ergun's drag force term by the temperature-dependent factor $(T/T_0)^{\omega}$ and Denton's heat-transfer coefficient by a factor of 2. For the reference temperature T_0 a value of 300 K, for the exponent ω a value of 1.0 has been chosen. The fact that the original correlations have to be altered, using either the rough first or the more sophisticated second possibility, may essentially be due to the unsteady and non-isothermal behavior of the flow.

4. CONCLUSIONS

The experimental work has shown that in front of the solid matrix a first strong reflection of the shock wave is followed by various weaker shock waves which lead to an acceleration of the reflected shock and to a continuous pressure increase in this region. Remarkable is the strong effect of the boundary layer along the front part of the cylinders in the first rows of the matrix. Between the cylinders a supersonic jet is formed which leads to a bow shock wave in front of the next cylinder. In the later phase a fully turbulent flow regime with essentially no wave phenomena is established.

In the numerical computations drag and heat-transfer laws of different authors were varied systematically. It was found that in the unsteady and non-isothermal case considered acceptable agreement between computational results and measured pressure profiles can only be achieved by modifications of the empirical correlations available. Therefore, two different modifications of these correlations are presented, both leading to qualitatively similar results. In the first case both Ergun's flow-resistance law [1] and Yoshida's heat-transfer correlation [8] have been modified by a constant factor. In the second case, Ergun's drag coefficient has been multiplied by a temperature dependent factor, whereas Denton's heat-transfer coefficient [7] has been doubled. The results obtained clearly show that there is a lack of knowledge about flow resistance in packed beds in the case of unsteady and non-isothermal flow with a large temperature difference between gas and solid phase. Particularly the drag in the hotter flow regions exceeds the drag predicted by the flow resistance correlations. Furthermore the results indicate that more extensive studies on the heat transfer in packed beds are necessary, especially in the case of high Reynolds numbers.

REFERENCES

1. S. Ergun, Fluid flow through packed columns, *Chem. Engng Prog.* **48**, 89–94 (1952).
2. H. Brauer, Eigenschaften der Zweiphasenströmung bei der Rektifikation in Füllkörpersäulen, *Dechema-Monographien* **37**, 7–78 (1960).
3. K. K. Kuo and C. C. Nydegger, Flow resistance measurement and correlation in a packed bed of WC 870 ball propellants, *J. Ballist.* **2**, 1–26 (1978).
4. D. P. Jones and H. Krier, Gas flow resistance measurements through packed beds at high Reynolds numbers, *Trans. Am. Soc. mech. Engrs* **105**, 168–173 (1983).
5. A. P. Colburn, Heat transfer and pressure drop in empty, baffled and packed tubes, *Ind. Engng Chem.* **23**, 910–923 (1931).
6. B. W. Gamson, Fluid solid systems, *Chem. Engng Prog.* **47**, 19–28 (1951).
7. W. H. Denton, *The Heat Transfer and Flow Resistance for Fluid Flow Through Randomly Packed Spheres*, p. 370. The Institution of Mechanical Engineers, London (1951).
8. F. Yoshida, D. Ramaswami and O. A. Hougen, Temperatures and partial pressures at the surface of catalyst particles, *A.I.Ch.E. Jl* **8**, 5–11 (1962).
9. V. Gnielinski, Gleichungen zur Berechnung des Wärme- und Stoffaustausches in durchströmten ruhenden Kugelschüttungen bei mittleren und großen Pecletzahlen, *vt "verfahrenstechnik"* **12**, 363–366 (1978).
10. W. Heilig and H. Reichenbach, Measurements of the unsteady drag coefficient of a circular cylinder, *Sixième Symposium Internationale sur Les Applications Militaires de la Simulation de Souffle*, première partie, Cahors (France) (1979).
11. W. Heilig, Air blast loading of a cylindrical body, *Int. Symposium on Flow Visualisation*, Bochum, F.R.G., pp. 544–549 (1980).
12. N. Zloch, Abschwächung von Verdichtungsstößen infolge Reibungswirkungen und Wärmeübergang bei vollausgebildeter turbulenter Strömung. Ph.D. thesis, Technische Hochschule Darmstadt (1974).
13. G. B. Wallis, *One-dimensional Two-phase Flow*. McGraw-Hill, New York (1969).
14. M. J. Zucrow and J. D. Hoffman, *Gasdynamics*, Vol. 2. John Wiley, New York (1976).
15. R. B. Bird, W. E. Stewart and E. N. Lightfoot, *Transport Phenomena*. John Wiley, New York (1960).
16. O. Laporte, On the interaction of a shock with a constriction, Los Alamos Science Lab., University of California, Report No. LA-1740 (1954).
17. H. Brauer, *Grundlagen der Einphasen- und Mehrphasenströmungen*, p. 429. Sauerländer, Aarau (1971).
18. E. R. G. Eckert and R. M. Drake, *Heat and Mass Transfer*, 2nd edn, p. 253. McGraw-Hill, New York (1959).
19. H. Krier and S. Rajan, Flame spreading and combustion in packed beds of propellant grains, AIAA 13th Aerospace Sciences Meeting, No. 75-240 (1975).

ECOULEMENT INDUIT PAR UN CHOC DANS UN ARRANGEMENT REGULIER DE CYLINDRES ET DES LITS FIXES

Résumé—On étudie expérimentalement et numériquement l'écoulement induit par un choc dans une matrice solide correspondant soit à un lit fixe de boulets sphériques soit d'un arrangement de cylindres perpendiculaires à l'écoulement. Les expériences sont réalisées dans un tube à choc en mesurant les profils de pression devant et à l'intérieur de la matrice. Une information qualitative sur la configuration de l'écoulement dans l'arrangement de cylindres est obtenue à partir de la méthode des ombres. Dans les calculs numériques, plusieurs lois de trainée et de transfert thermique sont vérifiées. Des essais d'ajustement de ces formules sont faits pour ajuster les résultats numériques aux données expérimentales.

DURCH STOSSWELLEN INDUZIERTE STRÖMUNG IN REGELMÄSSIGEN ZYLINDERANORDNUNGEN UND FESTBETTEN

Zusammenfassung—Die durch eine Stoßwelle induzierte Strömung in einem Festbett und in einer quer zur Strömungsrichtung ausgerichteten Zylinderanordnung wird experimentell und numerisch untersucht. Die Experimente werden in einem Stoßwellenrohr durchgeführt, wobei die Druckverteilung vor und zwischen den Hindernissen gemessen wird. Schattenaufnahmen des Strömungsfeldes in der Zylinderanordnung vermitteln qualitative optische Informationen. Bei den numerischen Rechnungen werden verschiedene Widerstands- und Wärmeübergangsgesetze getestet. Es werden Anpassungen dieser Korrelationen gemacht, um eine Übereinstimmung der numerischen und experimentellen Ergebnisse zu erzielen.

ТЕЧЕНИЯ В РЕГУЛЯРНОМ ПУЧКЕ ЦИЛИНДРОВ И ПЛОТНЫХ СЛОЯХ, ВЫЗВАННЫЕ УДАРОМ

Аннотация—Численно и экспериментально исследуется вызванное ударом течение в твердой матрице, состоящей либо из плотного слоя сферических гранул, либо пучка цилиндров, перпендикулярно расположенных по отношению к потоку. Эксперименты проводились в ударной трубе, при этом измерялись профили давления перед твердой матрицей и внутри нее. С помощью теневых приборов получены качественные данные по режиму течения в пучке цилиндров. При проведении численных расчетов использовались различные закономерности изменения сопротивления и теплообмена. Проводилась периодическая проверка этих соотношений на соответствие численных результатов экспериментальным данным.